JOURNAL OF GEOPHYSICAL RESEARCH, VOL. 113, C07053, doi:10.1029/2007JC004632, 2008

Modelling the formation and the long-term behavior of rip channel systems from the deformation of a longshore bar

Roland Garnier,[1] Daniel Calvete,[2] Albert Falqués,[2] and Nicholas Dodd[1]

Received 9 November 2007; revised 21 February 2008; accepted 7 April 2008; published 31 July 2008.

[1] A nonlinear numerical model based on a wave- and depth-averaged shallow water equation solver with wave driver, sediment transport, and bed updating is used to investigate the long-term evolution of rip channel systems appearing from the deformation of a longshore bar. Linear and nonlinear regimes in the morphological evolution have been studied. In the linear regime, a crescentic bar system emerges as a free instability. In the nonlinear regime, merging/splitting in bars and saturation of the growth are obtained. In spite of excluding undertow and wave-asymmetry sediment transport, the initial crescentic bar system reorganizes to form a large-scale and shore-attached transverse or oblique bar system, which is found to be a dynamical equilibrium state of the beach system. Thus the basic morphological transitions "Longshore Bar and Trough" → "Rhythmic Bar and Beach" → "Transverse Bar and Rip" described by earlier conceptual models are here reproduced. The study of the physical mechanisms allows us to understand the role of the different transport modes: The advective part induces the formation of crescentic bars and megacusps, and the bedslope transport damps the instability. Both terms contribute to the attachment of the megacusps to the crescentic bars. Depending on the wave forcing, the bar wavelength ranges between 180 and 250 m (165 and 320 m) in the linear (nonlinear) regime.

Citation: Garnier, R., D. Calvete, A. Falqués, and N. Dodd (2008), Modelling the formation and the long-term behavior of rip channel systems from the deformation of a longshore bar, *J. Geophys. Res.*, *113*, C07053, doi:10.1029/2007JC004632.

1. Introduction

1.1. Rip Channel Systems

[2] Many text books on coastal sciences rely on the simple concept of equilibrium beach profile as a cross-shore bathymetric profile which is invariant along the shore (at least at the length scale of a few times the surf zone width [see, e.g., *Komar*, 1998]). However, present systematic and careful observations reveal that rather than being the rule this is an exception or maybe just a long-term average [*Short*, 1999; *van Enckevort et al.*, 2004; *Castelle et al.*, 2007; *Ribas and Kroon*, 2007]. In fact, the nearshore in front of sandy beaches very often exhibits complex bathymetric patterns with bars, shoals, troughs, channels and holes. As a result, the cross-shore profiles at distinct cross sections of the same beach may be very different.

[3] The most simple of such bathymetric features are breaker bars which are shore parallel, straight in plan view and with the bed level at their crest being approximately constant alongshore [*Komar*, 1998; *Short*, 1999]. However, the bed level at the bar may also be alongshore oscillating in such a way that wide shallow sections alternate with narrow deep sections, so-called rip channels. The most important feature of such channels is that breaking waves force strong jet-like currents in them which are seaward directed and called rip currents. In many cases, when rip channels are present the bar is no longer straight in plan view, but meandering, so that the deepest sections are shifted offshore and the shallowest sections are shifted onshore. Such bars are called crescentic [*van Enckevort et al.*, 2004; *Lafon et al.*, 2004, 2005; *Castelle et al.*, 2007; *Ruessink et al.*, 2007]. The alongshore wavelength of the undulations in plan view (or the spacing between rip channels) is of the order of a few times the distance of the bar to the shore and may be quite regular (although not always). For this reason, such bathymetric patterns are known as rhythmic topography.

[4] Surf zone bars that are not parallel to the coast but form a certain angle with it have also been described and are generically known as transverse bars. More specifically, the term "transverse" is used when the bars are shore-normal and the term "oblique" is used instead when the bars form an angle between 0 and 90° with the shore normal. Several such bars may appear along the coast with a spacing of the order of one to a few times the surf zone width. Again, the spacing may be quite regular so that the pattern is also known as rhythmic topography. In many cases, the bars are connected to a shore with a cuspate shoreline, the cusps (megacusps) being associated with the bar attachments [*Evans*, 1938; *Komar*, 1998; *Short*, 1999].

[5] While crescentic bars seem to be associated to a preexisting straight bar, the origin of transverse bars is not

[1] School of Civil Engineering, University of Nottingham, Nottingham, UK.
[2] Departament de Física Aplicada, Universitat Politécnica de Catalunya, Barcelona, Spain.

0148-0227/08/2007JC004632$09.00

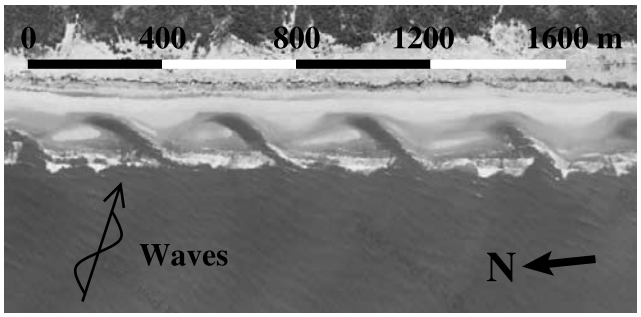

(a) Large scale oblique bars

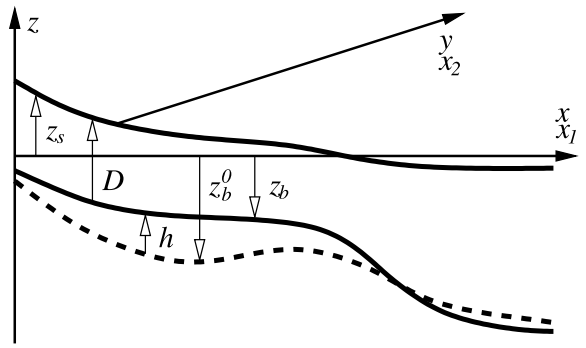

(b) Coordinate system

Figure 1. (a) Large-scale oblique bars (sometimes called ridge and runnel system). French Aquitanian coast. IGN Paris 2007. (b) Coordinate system. The x, y, and z axes (x_1, x_2, and x_3 axis, respectively) stand for the cross-shore, the longshore, and the vertical directions, respectively. The coastline is at $x = 0$. z_s is the sea level, D is the water depth, h is the bottom perturbation with respect to the longitudinally uniform initial topography, z_b^0 is the initial bed level, and z_b is the bed level.

so clear and there are several types. A well defined class are the shoals that develop from the shallowest sections of a crescentic bar that progresses onshore until they attach to the shoreline. This process and the corresponding morphology was described by *Wright and Short* [1984] in the case of single-barred systems in macrotidal, wave-dominated environments with relatively small bars and is essential to their "TBR" ("Transverse Bar and Rip") beach state. The bars may be exactly shore-normal or slightly oblique. We will refer to them as "large-scale transverse bars" [*MacMahan et al.*, 2005; *Castelle et al.*, 2007]. Another type are the intertidal oblique bars, which are very common along the French Aquitanian coast [*Lafon et al.*, 2002, 2004, 2005; *De Melo Apoluceno et al.*, 2002; *Castelle et al.*, 2007]. They were previously called "ridge and runnel systems" since they appear in the intertidal zone. However, they differ from the typical ridge and runnel systems described for instance in *Short* [1999]; *Kroon and Masselink* [2002]; *Masselink and Kroon* [2006], because, in particular, (1) they exhibit a clear alongshore rhythmicity and (2) the crests are separated by a deep channel. They are actually similar to the large-scale transverse bars except that they show an oblique downcurrent orientation, i.e., they appear skewed down current when viewed from the shore (Figure 1a). They will be referred to as "large-scale oblique bars". In this paper we consider these two types of transverse/oblique bars that we call "large scale", to distinguish them from a third type that has been called "transverse/oblique finger bars" by *Ribas and Kroon* [2007], and was previously described by *Niederoda and Tanner* [1970]; *Falqués* [1989]; *Komar* [1998]; *Konicki and Holman* [2000]. These are thin and elongated offshore, and the spacing between them is smaller.

[6] Although the existing literature set up a clear classification of all these features [*Komar*, 1998] improvement in observation techniques (e.g., Argus System) and the onset of mathematical morphodynamical models reveals that: i) the old classification is overwhelmed by the increasing complexity of observations that suggests more types and subtypes than previously foreseen; and ii) different morphologies can be genetically linked, as they are different stages of the same morphodynamical process. Nevertheless, a common characteristic of all these surf zone bathymetric patterns that are alongshore rhythmic (or quasi-rhythmic) is the alongshore succession of shoals and deeps, with breaking waves forcing rip currents at the deeps. Thus we will refer generically to such systems as "rip channel systems".

1.2. Modelling Rip Channel Systems

[7] The origin of rip channel systems was attributed in the past to the hydrodynamical forcing by infragravity edge waves [*Bowen and Inman*, 1971; *Holman and Bowen*, 1982]. However, it has been more recently found that positive feedbacks between waves, currents and morphology may render unstable an alongshore uniform surf zone and may thus lead to the formation of rhythmic topography. Even if the hydrodynamic forcing could have some influence as an initial triggering of those instabilities, the actual shape of the bathymetric patterns is eventually dominated by those feedbacks. This has been shown by numerous modelling studies regarding the different types of bars during the last decade. For example, the formation of rip channel systems and transverse/oblique bars in planar beaches (i.e., unbarred) has been examined by *Christensen et al.* [1994]; *Falqués et al.* [1996, 2000]; *Caballeria et al.* [2002]; *Ribas et al.* [2003] and *van Leeuwen et al.* [2006]. The tendency of a straight shore parallel bar to develop rip channels and to become crescentic has been investigated by *Deigaard et al.* [1999]; *Damgaard et al.* [2002]; *Reniers et al.* [2004]; *Calvete et al.* [2005, 2007]; *Dronen and Deigaard* [2007]; *Klein and Schuttelaars* [2006], the latter study actually dealing with a double barred system.

[8] Many of these studies use linear stability analysis to investigate the tendency to form rip channels from an initial featureless beach and to elucidate the nature of the feedback that is behind this process. To track the actual growth of the rip channel systems up to an amplitude comparable with natural systems a nonlinear stability analysis is necessary and this is done in some of those studies. However, none of them is able to run for a long time, i.e., more than a few times the typical growth time. Usually, the models break

down before or just when the amplitude of the bars is comparable to that observed in nature [*Caballeria et al.*, 2002; *Dronen and Deigaard*, 2007]. In other models the water depth above the bar crest keeps on decreasing until zero and the model breaks down at this moment [*Damgaard et al.*, 2002]. As a consequence, none of these models can describe the long-term behavior of the system and for this reason they cannot describe the "finite amplitude dynamics" and in particular, the transitions from one type of rhythmic system to another.

[9] However, *Garnier et al.* [2006a] have recently shown that an adequate treatment of the gravitational downslope sediment transport together with a simplified description of wave refraction allows for long-term runs (∼100 day or more) of the morphodynamical nonlinear stability model MORFO55. The model is able to describe the formation, the saturation of the growth and the finite amplitude dynamics of transverse/oblique bars on a planar beach and, despite the simplifications, model results are fairly consistent with observations. Preliminary computations for a barred beach have shown that the model may also predict the formation of large-scale oblique bars from an initially straight bar, which becomes crescentic and further evolves into the transverse/oblique bar system *Garnier et al.* [2006b]. This is one of the basic transitions described by *Wright and Short* [1984] ("RBB" → TBR, i.e., "Rhythmic Bar and Beach" to Transverse Bar and Rip morphology), and conceptual models had been presented by *De Melo Apoluceno* [2002]; *Castelle et al.* [2007]. The first modelling study has been made by *Ranasinghe et al.* [2004] who reproduce the RBB → TBR transition of an event in Palm Beach, Australia. In agreement with the observation, their numerical simulations show that this transition can occur for reduced incident wave conditions that follow a stronger event when the RBB state formed. However, their initial topography is based on a preexisting RBB state given by Argus images and their model was unable to reach this state.

1.3. Objectives

[10] The aim of the present contribution is to conduct a systematic nonlinear instability analysis of a single-barred beach by using the MORFO55 model. The objectives are: (1) properties of the saturation and nonlinear dynamics. In particular, quantification of the amplitude, existence of a new (dynamical?) equilibrium and systematic modelling of the RBB → TBR transition that was initiated in *Garnier et al.* [2006b], and (2) comparison of the initial formation of a crescentic bar with the linear stability studies of *Calvete et al.* [2005]. In particular, possible formation of megacusps and transverse bars at the shore coupled with the crescentic bar.

[11] This paper is organized as follows: section 2 is dedicated to a description of the model and of the experimental setup, section 3 presents the main results; the physical mechanisms are explained in section 4, and finally an overall discussion and a conclusion are given in sections 5 and 6, respectively.

2. Numerical Model

2.1. Set of Equations

[12] The MORFO55 model is based on the phase-averaged nonlinear shallow water equations [*Mei*, 1989; *Garnier et al.*, 2006a]. It is applied to a rectilinear beach defined by the coordinate system (O, x, y, z), or (O, x_1, x_2, x_3), where [O, x) stands for the positive seaward cross-shore direction, [O, y), for the longshore direction and [O,z), for the positive upward vertical direction (see Figure 1b). The set of six wave and depth-averaged equations comprises the water mass conservation equation (1), the momentum conservation equation (2), the wave energy equation (3), the Snell's law (4) and the sediment mass conservation equation (5). They read (repeated indices indicate summation with i, j = 1, 2; t is time):

$$\frac{\partial D}{\partial t}+\frac{\partial}{\partial x_j}\left(D\,v_j\right)=0\ , \tag{1}$$

$$\frac{\partial v_i}{\partial t}+v_j\frac{\partial v_i}{\partial x_j}=-g\frac{\partial z_s}{\partial x_i}-\frac{1}{\rho D}\frac{\partial}{\partial x_j}\left(S'_{ij}-S''_{ij}\right)-\frac{\tau_{bi}}{\rho D}\ , \tag{2}$$

$$\frac{\partial E}{\partial t}+\frac{\partial}{\partial x_j}\left(\left(v_j+c_{gj}\right)E\right)+S'_{ij}\frac{\partial v_j}{\partial x_i}=-\varepsilon\ , \tag{3}$$

$$k\,\sin\theta=k^0\,\sin\theta^0\ , \tag{4}$$

$$\frac{\partial z_b}{\partial t}+\frac{\partial q_j}{\partial x_j}=0\ . \tag{5}$$

[13] The six time- and depth-averaged dynamical unknowns are: the sea level $z_s(x_1, x_2, t)$, the two components u and v (v_1 and v_2, respectively) of the horizontal velocity $\vec{v}$ (x_1, x_2, t), the wave energy density $E(x_1, x_2, t)$, the wave angle $\theta(x_1, x_2, t)$ and the bed level $z_b(x_1, x_2, t)$.

[14] The other variables are defined as follows. D is the total mean depth ($D = z_s - z_b$). g is the acceleration due to gravity (g = 9.8 m s^{-2}). ρ the water density (ρ = 1024 kg m^{-3}). S' is the wave radiation stress tensor from *Longuet-Higgins and Stewart* [1964]. S'' is the turbulent Reynolds stress tensor [*Battjes*, 1975]. τ_b is the bed shear stress vector [*Mei*, 1989; *Garnier*, 2007].

[15] The relationship between the wave energy E and the root mean square wave height H_{rms} is given by: $E = \rho\, g\, H_{rms}^2/8$. $\vec{c_g}$ is the group velocity vector. ε is the dissipation rate because of wave breaking [*Thornton and Guza*, 1983] and bottom friction [*Horikawa*, 1988; *Garnier et al.*, 2006a].

[16] In the Snell's law (4), the wave number k is the modulus of the wave vector $\vec{k}$ and is computed using the dispersion relation, θ is defined as the angle between the wave rays and the x axis, k^0 and θ^0 are the wave number and the wave angle at the seaward boundary. Notice that by using this approximation, the wave topography interaction because of wave refraction are not taken into account. This seems to be correct as the results by using the Eikonal equation do not essentially change. However, we decide to keep the Snell's law in order to simplify the equation system and focus on the main mechanisms at the origin of the beach instability.

[17] The horizontal sediment flux vector is based on the total load formula of Soulsby and Van Rijn [*Soulsby*, 1997]

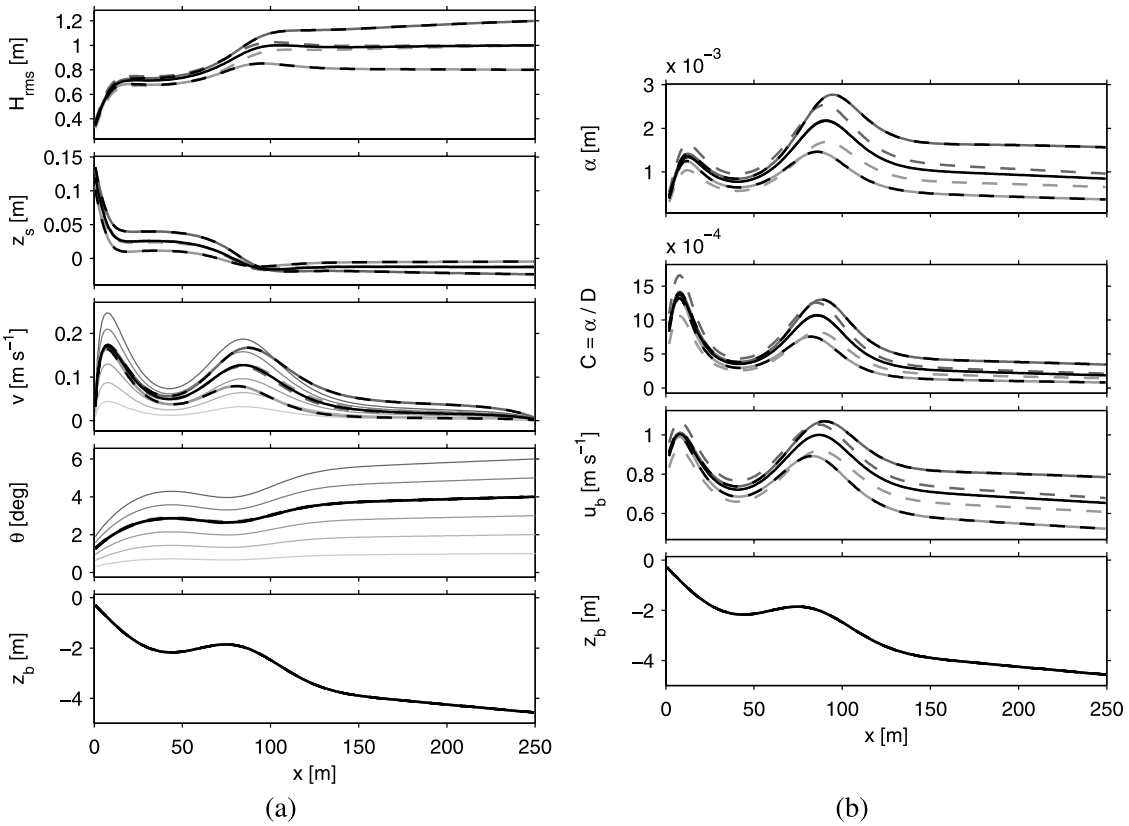

Figure 2. Basic states. Cross-shore profiles at the longitudinally uniform equilibrium state obtained in the case of nonperturbed initial topography (oblique wave incidence). Black thick line: default case. Dashed gray line: variation of wave period. Dashed black/gray line: variation of incident wave height. Gray line: variation of incident wave angle. (a) Hydrodynamical variables: root mean square wave height $H_{\rm rms}$, sea level $z_{\rm s}$, cross-shore velocity v, wave angle θ, and bed level $z_{\rm b}$. (b) Morphodynamical variables: stirring factor α, potential stirring C, root mean square wave orbital velocity amplitude at the bottom $u_{\rm b}$, and bed level $z_{\rm b}$.

(see details in *Calvete et al.* [2005] and *Garnier et al.* [2006a]). It reads:

$$\vec{q} = \alpha\left(\vec{v} - \gamma\, u_{\rm b}\, \vec{\nabla} h\right) \ , \tag{6}$$

where α is the stirring factor, γ is the bedslope coefficient, $u_{\rm b}$ is the root mean square wave orbital velocity amplitude at the bottom and h is the bed level deviation from initial equilibrium ($h = z_{\rm b} - z_{\rm b}^0$, where $z_{\rm b}^0$ is the initial bed level, see Figure 1b). In order to simplify the notations, the bed porosity $p = 0.4$ has been included in α:

$$\begin{aligned} \alpha &= \frac{1}{1-p}\, A_{\rm S}\, (u_{\rm s} - u_{\rm c})^{2.4} \quad \text{if } u_{\rm s} > u_{\rm c} \\ &= 0 \qquad\qquad\qquad\qquad\quad \text{otherwise,} \end{aligned}$$

where $A_{\rm s}$ and $u_{\rm c}$ depend essentially on sediment characteristics and water depth [*Soulsby*, 1997]. The stirring velocity $u_{\rm s}$ reads:

$$u_{\rm s} = \left(|\vec{v}|^2 + \frac{0.018}{c_{\rm D}}\, u_{\rm b}^2 \right)^{1/2} ,$$

$c_{\rm D}$ being the morphodynamical drag coefficient [*Soulsby*, 1997].

[18] There is an important degree of uncertainty in the value of the bedslope coefficient γ [*Garnier et al.*, 2006a]. In the model it is chosen so as to have realistic results and to perform long-term evolutions. Here, it is fixed to $\gamma = 5$ which is higher than the default case of *Garnier et al.* [2006a] ($\gamma = 1.5$). With $\gamma = 1.5$, the large-scale instabilities obtained here end up in an area that is too shallow close to the shoreline leading to negative depth and model overflow. Since it depends on the mean current $\vec{v}$ and on the bed perturbation h, the onshore transport driven by wave nonlinearity and undertow is excluded. In fact, this onshore transport is assumed to be in balance with the gravitational downslope transport which takes into account the total beach slope ($\vec{\nabla} z_{\rm b}$). The stirring factor α depends essentially on the water depth, on the current velocity magnitude, on $u_{\rm b}$ and on the sediment characteristics. In particular, the sediment grain size has been chosen as $D_{50} = 0.25$ mm and the bed roughness length as $z_o = 6$ mm.

[19] Periodic boundary conditions for each variable and for its first y derivative are applied at the lateral boundaries. For more details on the offshore and shoreline boundary

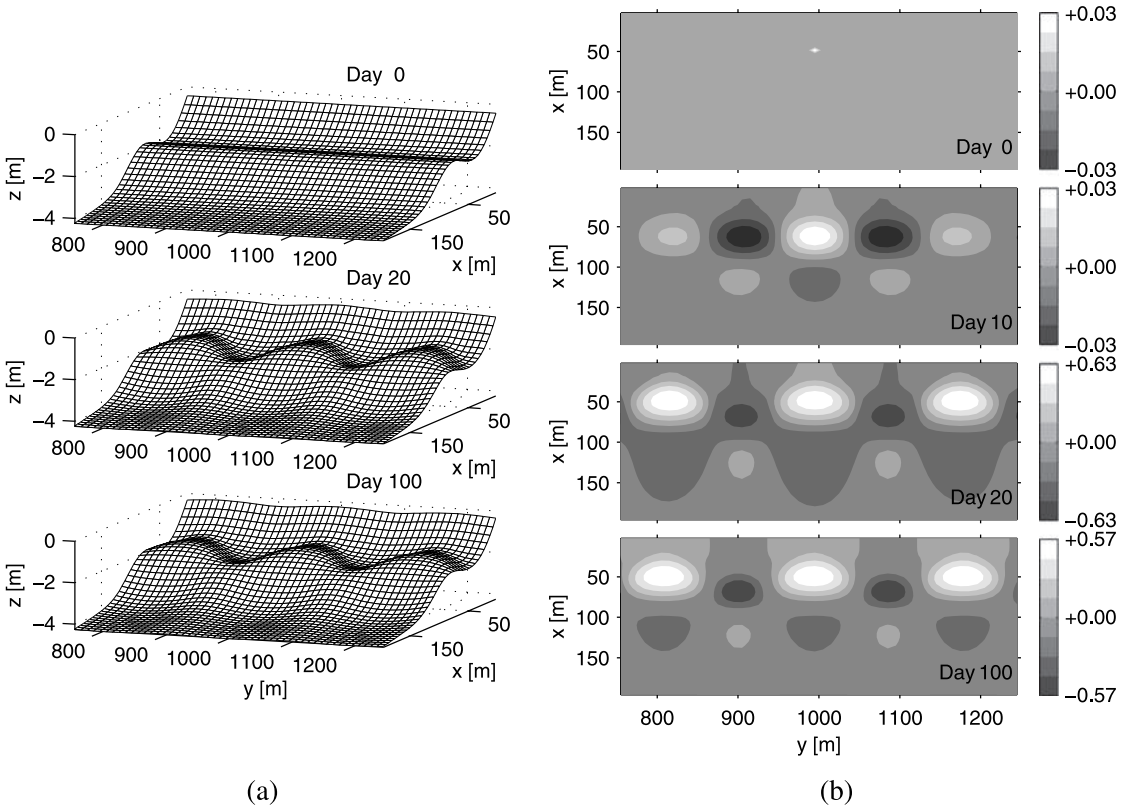

Figure 3. Normal wave incidence. Snapshots of a part of the topography during the formation, development, and growth saturation of crescentic bar system. (a) Tridimensional view of the bed level z_b. (b) Top view of the bottom perturbation h (in meters).

conditions and on the numerical methods, please refer to *Garnier et al.* [2006a] and *Garnier* [2007].

2.2. Setup of the Numerical Simulations

[20] The initial topography is assumed to be a longitudinally uniform longshore barred beach where a small perturbation has been added. Thus the initial topography can be written as:

$$z_b(x,y,t=0) = z_b^0(x) + h(x,y,t=0)\ . \tag{7}$$

[21] The initial equilibrium barred beach profile $z_b^0(x)$ is based on the bar system at Duck, North Carolina [*Yu and Slinn*, 2003]:

$$z_b^0(x) = -a_0 - a_1\left(1-\frac{\beta_2}{\beta_1}\right)\tanh\left(\frac{\beta_1 x}{a_1}\right) - \beta_2 x + a_2 \exp\left[-5\left(\frac{x-x_c}{x_c}\right)^2\right]\ , \tag{8}$$

where x_c is the bar location (x_c = 80 m) and a_2 is the bar amplitude (default case: a_2 = 1.5 m). The height of the water depth at the swash/surf zone boundary is a_0 = 25 cm and a_1 = 2.97 m. The shoreline and offshore slopes are β_1 = 0.075 and β_2 = 0.0064, respectively. The bottom plot of Figures 2a and 2b show the equilibrium profile $z_b^0(x)$ while the top plot of Figure 3a shows the three-dimensional view of a part of the initial bathymetry $z_b(x, y, t = 0)$. The same profile has been used in the linear stability analysis of *Calvete et al.* [2005], which provides a useful tool for validating our initial results.

[22] The initial perturbation $h(x, y, t = 0)$ is a Dirac delta function in order to not excite preferentially a particular mode. It has been fixed at: $h(x = 50$ m, $y = 1000$ m, $t = 0) =$ 3 cm and $h(x \neq 50$ m, $y \neq 1000$ m, $t = 0) = 0$. Notice that the growth rate of the emerging instabilities does not depend either on the location, or on the amplitude of the local peak.

[23] Experiments have been done on the domain defined by: $0 \leq x \leq L_x = 250$ m and $0 \leq y \leq L_y = 2000$ m. The grid spacing is given by $(\Delta x, \Delta y) = (5, 10)$ m. The hydrodynamical time step $\Delta t = 0.05$ s. The morphodynamical processes have been artificially accelerated by a factor 90 [see *Caballeria et al.*, 2002; *Garnier et al.*, 2006a] so that the morphodynamical time step is $\Delta t_m = 90\ \Delta t = 4.60$ s. Notice that the use of a factor 1 does not change the initial growth rate of the instabilities, and the entire evolution is the same by using a factor from 50 to 150. Results are given up to 300 days of morphological evolution.

[24] Two reference cases are described: (1) for normal wave incidence and (2) for oblique wave incidence with a wave angle of $\theta(L_x, y, t) = \theta^0 = 4°$ at the seaward boundary (in 4.5 m depth). The height of incident waves $H_{rms}(L_x, y, t) = H_{rms}^0 = 1$ m at the seaward boundary and the wave period $T = 6$ s.

2.3. Basic States

[25] In the absence of an initial perturbation, i.e., if the initial topography is exactly alongshore uniform ($h(x, y, t = 0) = 0$), the initial topography remains constant. After 50 min of beach evolution, an hydrodynamical equilibrium state is reached called the ''basic state''. Figure 2a shows the cross-shore profile of the (alongshore uniform) hydrodynamical variables at the basic state for oblique waves, where the bottom plot is the bed profile. As the H_{rms} plot shows, most of wave breaking occurs firstly when waves starting from x = 250 m arrive over the longshore bar (x = 80 m) and secondly in the inner surf zone (x = 10 m), these two cross-shore locations are marked by two strong increases in wave setup (z_s) and by two peaks in the longshore current profile ($v = 0.12$ m s^{-1} at x = 80 m and $v = 0.16$ m s^{-1} at x = 10 m for the default case). Notice that the cross-shore velocity is not plotted because it vanishes. The wave angle stops decreasing and even increases from the top of the bar up to the inner trough. The morphodynamical variables are plotted in Figure 2b, where both α and α/D profiles presents two peaks at the aforementioned cross-shore locations. In particular the profile of the latter variable also called the ''potential stirring'' and interpreted as a depth-averaged sediment concentration (we will denote it $C = \alpha/D$) is important for interpreting the formation of rhythmic features [*Falqués et al.*, 2000; *Caballeria et al.*, 2002; *Ribas et al.*, 2003; *Calvete et al.*, 2005; *Garnier et al.*, 2006a]. The presence of these two maxima could explain the emergence of two kinds of rhythmic features around the peak locations: smaller features around the inner peak (transverse bars), and larger features around the outer peak (crescentic bars). The smaller features have been specifically studied in *Garnier et al.* [2006a] by excluding the longshore parallel bar, in which case the outer peak in the C profile is removed. The small-scale transverse bars do not appear with the present beach configuration for the three following reasons. Firstly the height of incoming waves in the inner surf zone is strongly reduced because of the presence of the longshore bar. Secondly, they are not well resolved because of the large grid spacing that damps small-scale features, in particular, the present longshore grid spacing is only one third of the distance between two small-scale transverse bars. Thirdly the present value of the bedslope coefficient: $\gamma = 5$, is out of range for the emergence of these features which cannot appear for $\gamma > 2.5$. The interaction between these two kinds of features has been investigated in *Garnier* [2007b] showing the necessity to implement a moving shoreline in order to find an equilibrium beach configuration.

3. Results

3.1. Normal Wave Incidence

[26] For normal wave incidence, as predicted by previous modelling studies, crescentic patterns appear from a deformation of the longshore bar. From the initial time up to day 100, Figures 3a and 3b) shows snapshots of the bed level (z_b) and of the bottom perturbation (h). At day 0, the initial perturbation is displayed. A series of bumps (troughs) appear on the shoreward part of the longshore bar with a sinusoidal shape (day 10) and extend seaward with less developed troughs (bump). We will distinguish the bar system appearing shoreward of the top of the initial longshore bar from the antiphase bar system appearing seaward by calling them the 'inner' system and the 'outer' system, respectively. At day 20, crescentic bars have reached a maximum amplitude ($A_m = 0.46$ m) and are slightly damped until day 100 ($A_m = 0.42$ m). At this time, we consider that the bars have reached an equilibrium state. Their shape differs from the initial state (day 10) as they display asymmetry: the inner (outer) shoals have a larger (smaller) longshore span than the inner (outer) troughs. Compared to the previous states, the cross-shore extension of the equilibrium crescentic system is larger. Interestingly, the inner structures extend onshore up to the shore boundary. A kind of large-scale transverse bar separated by narrow channels thus attaches itself to the shore, hinting at the possible formation of an undulating coastline. By examining Figure 3b the transition between a RBB state to a TBR state can be detected. At Day 10, the central bar is attached to the shore, while the lateral bars (y = 825 m and y = 1175 m) are not. Actually, the instabilities start to develop at the center of the domain, where the bottom is perturbed (Figure 3b, day 0), so at day 10 the perturbation is more evolved at the center compared to other area in the domain. Note that, at the equilibrium state (day 100), the bar system is alongshore periodic: the lateral bar evolution has caught up with the central bar.

[27] Figure 4e shows the current circulation on the total topography. A clear rip current system appears, jet-like offshore oriented in the inner channels and slightly wider over the inner crests. Its maximum magnitude is 0.30 m s^{-1}. From top to bottom, Figure 4f displays the mean sea level, the cross-shore and longshore components of the velocity vector and the bottom perturbation at the final state. Because of an increasing setup over the bars in the inner surf zone, the mean sea level and the inner bar system are in phase. Confirming the observation of the rip current system in Figure 4e, the cross-shore velocity u is in antiphase with the inner bar system. The cross-shore velocity is focused over the inner crescentic system. This latter seems to control the velocity field while the outer bar system does not seem to have effect on the current circulation. The longshore velocity v is also dominant over the inner bar system. The secondary circulation observed in laboratory experiments and numerical studies [*Haller et al.*, 2002; *Yu and Slinn*, 2003; *Calvete et al.*, 2005] that consists in a counterrotating system rip current system close to the shoreline is here weak compared to the main circulation.

[28] The time series presented in Figure 4a display the time evolution of the bed perturbation h along the longshore section defined by x = 50 m. The bars appear at day 5 and they reach an amplitude of 2 cm at day 10. The Fourier analysis of this section (Figure 4b) gives the intensity of the modes as a function of the bar spacing λ. From the formation of bars up to the final state, the maximum intensity occurs for $\lambda = \lambda_m = 180$ m (Figure 4c), where λ_m is called the predominant spacing. During the bar growth, the Fourier coefficient of the predominant mode exponentially grows, with a growth rate of $\sigma = \sigma_m = 0.58$ day^{-1} (σ_m is the predominant growth rate). Its inverse is called the e-folding time, which is $\tau = \tau_m = 1.72$ day. Notice that the e-folding time is different from the ''growth time'' which is about 20 days. The e-folding time does not depend on the initial perturbations and provides a more reliable

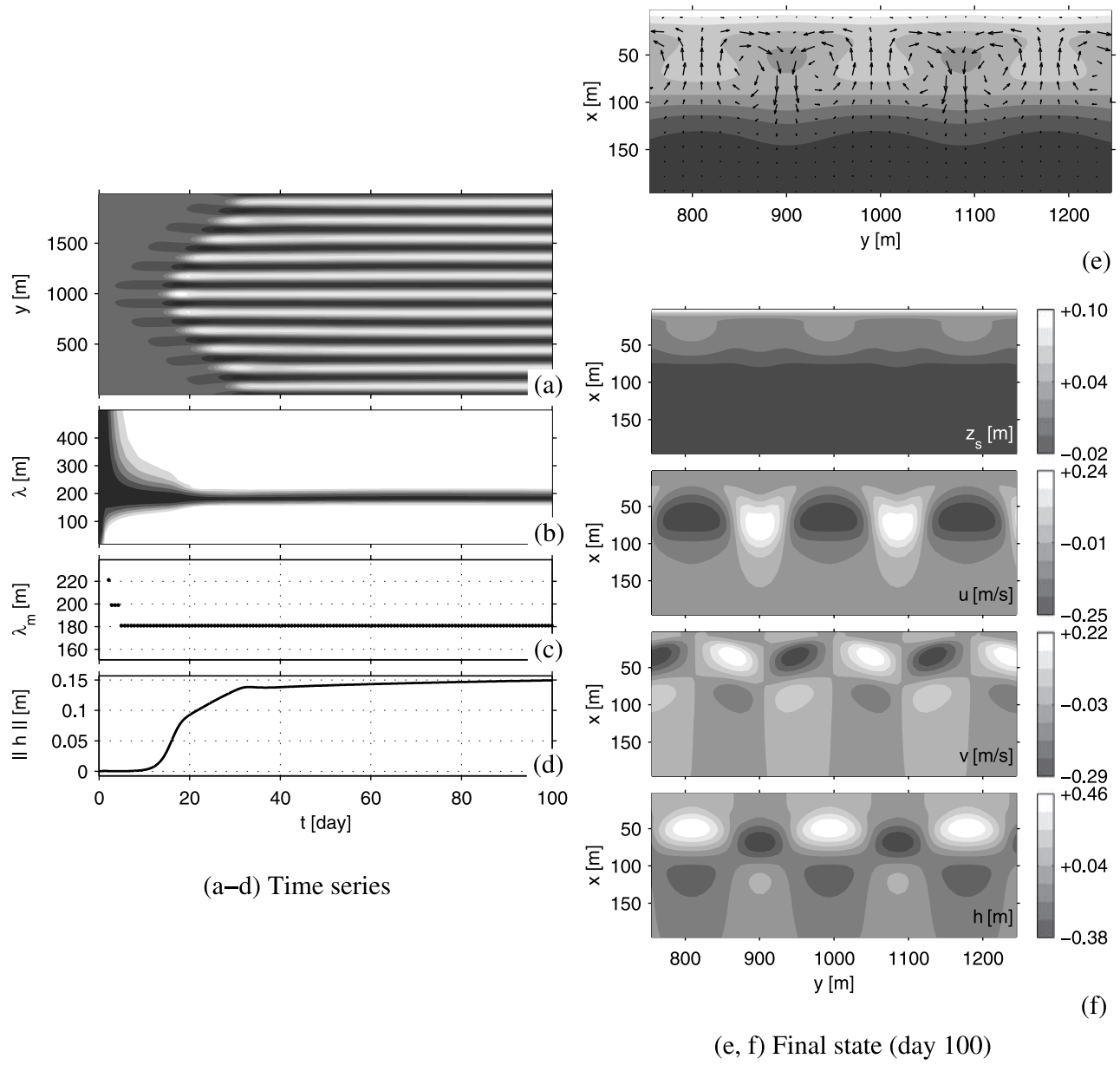

Figure 4. Normal wave incidence. Left: time series. From top to bottom: (a) $h(x = 50$ m, y, $t)$, the bed level along the longshore section $x = 50$ m, darker colors = deeper areas; (b) $F(x = 50$ m, λ, $t)$, its Fourier transform, darker colors = more unstable modes; (c) $\lambda_m(x = 50$ m, $t)$, the resulting predominant spacing; and (d) $\| h \|$ = representative of the bar amplitude. Right: final state (day 100). (e) Bathymetric contours (z_b) and circulation ($\vec{v}$) over crescentic bar systems. White = shallowest areas, shaded = deepest areas. Maximum current magnitude = 0.3 m s^{-1}. (f) From top to bottom: z_s, u, v, and h.

measure of the morphodynamical response time of the system.

3.2. Oblique Wave Incidence

[29] For oblique wave incidence ($\theta^0 = 4°$), crescentic patterns appear later, with an oblique orientation. Snapshots of the total topography and of the bed elevation are displayed in Figure 5. At day 15 (Figure 5b), the rhythmic system has the amplitude of $A = 1$ cm while for normal waves, crescentic bars had reached a large amplitude. At this time, they are reminiscent of the crescentic bars observed in the previous section, firstly because they have a similar wavelength, secondly because of the presence of an antiphase inner and outer bar system and thirdly because the inner system extends onshore up to the coastline. However the present system has an oblique orientation: the ambient longshore current direction coinciding with the y axis direction, the bar system is down current oriented in the inner part of the longshore bar, while it is up current oriented in the outer part. From day 15 to day 40, the dominating growth of the rhythmic system occurs in the inner zone. At day 100, the cross-shore location of the top of the crests is maintained in the inner part of the longshore

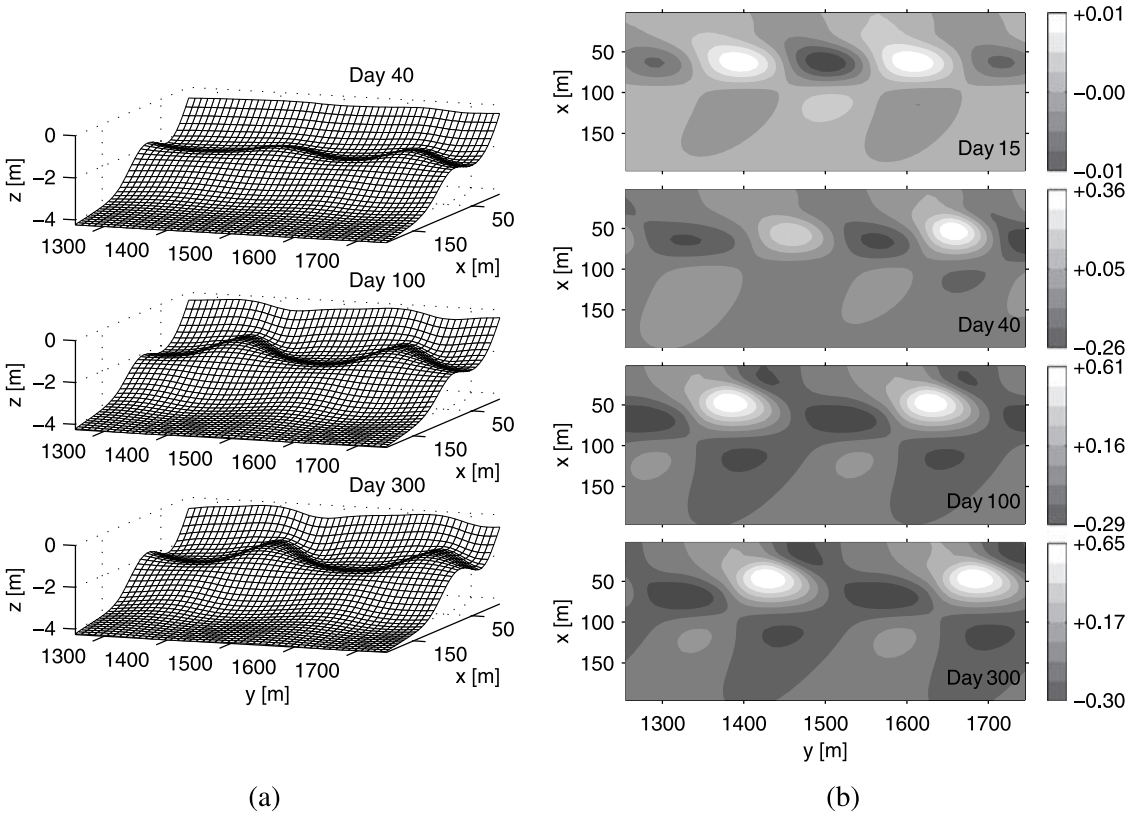

Figure 5. Oblique wave incidence. Snapshots of a part of the topography during the formation, development, and growth saturation of oblique crescentic bar or large-scale oblique bar system. (a) Tridimensional view of the bed level z_b. (b) Top view of the bottom perturbation h (in meters).

bar, however, the deepest area of the troughs occurs in two cross-shore locations: (1) close to the shoreline, somewhat down current of the crest and (2) in the inner part of the longshore bar, down current of (1). The former becomes deeper at the final state suggesting a strong undulation of the coastline with subdued shoals and deep troughs. The final rhythmic pattern is reminiscent of large-scale oblique bars with deep channels. They are attached to the shoreline and have an amplitude of A = 48 cm. The outer system is less pronounced and up current oriented.

[30] The total bathymetry and the current circulation at the final state are displayed in Figure 6a. The initially alongshore uniform longshore current is now deflected showing a strong rip current system (the maximum current magnitude is 0.4 m s^{-1}). The current is onshore deflected over the crest of the large-scale oblique bar system and is thrown offshore in the channel. By analyzing the sea level and each component of the current vector (Figure 6b), we notice the same kind of behavior as for normal waves (Figure 4e), in particular, at the final state, the current circulation has a full two-dimensional shape.

[31] Figures 7a–7d show a complex time evolution of the morphodynamical system. The initial mode seems to dominate until day 30, characterized by a predominant wavelength of λ_m = 220 m. The corresponding growth rate is σ_m = 0.24 day^{-1}, i.e., the e-folding time is τ_m = 4.16 day. Then, strong nonlinear behaviors of merging and splitting in bars appear. The predominant wavelength oscillates between 180 m $\leq \lambda_m \leq$ 250 m. In contrast to the previous result (Figures 4a–4d), the predominant wavelength does not quickly stabilize and seems to evolve periodically (with a period of about 50 days) up to day 300, when the oscillation seems eased and λ_m = 250 m. We do not pretend that this is a general result characteristic to the large-scale oblique bar evolution. It is more a particular result which has been obtained in some particular conditions. This illustrates the capability of the model to simulate strong nonlinear behaviors, and that an equilibrium state with a unique mode may be hard to be reached. As will be shown in the next section, the time to reach the equilibrium state may vary, depending on how much the bars split and merge. Figure 7a allows computations of the migration velocity of the bars. The initial velocity is $c_m \sim$30 m day^{-1} (corresponds to λ_m = 220 m) while the final one is $c_m \sim$14 m day^{-1} (corresponds to λ_m = 250 m). As in the study of *Garnier et al.* [2006a], the migration velocity is smaller for bars with larger sand volume.

3.3. Parametric Trends

[32] The influence of different wave conditions on the bar properties is examined. The results are reported in Table 1. The variation of the incident wave height H^0_{rms} and the wave period T by ±20% from the default value is considered (for normal and oblique waves). Moreover, we analyze the effect of different incident wave angles (up to θ^0 = 7°).

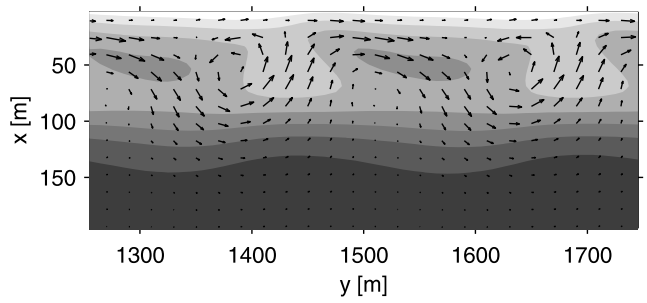

(a)

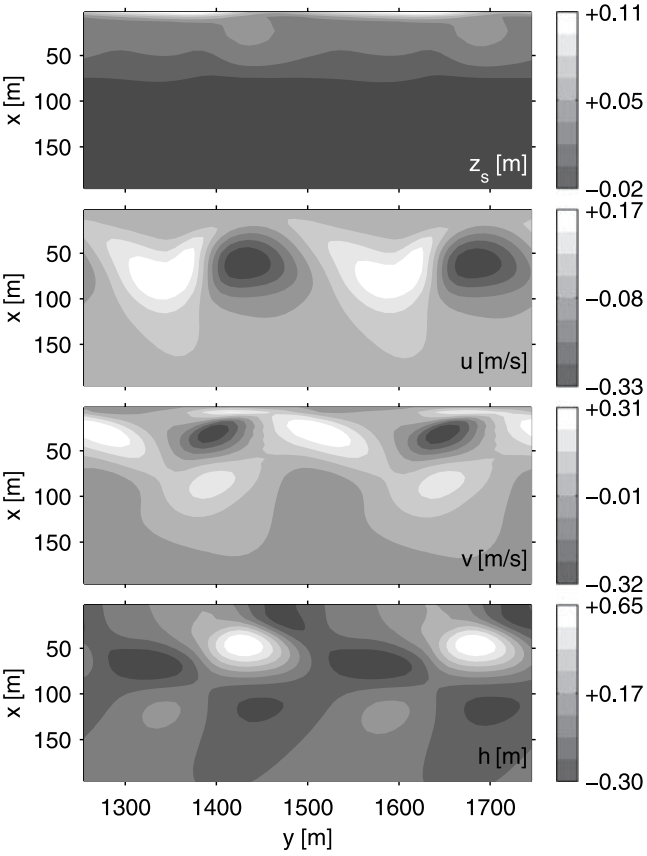

(b)

Figure 6. Oblique wave incidence. Final state (day 300). (a) Bathymetric contours (z_b) and circulation ($\vec{v}$). The shallowest areas are white, and the deepest areas are shaded. Maximum current magnitude: 0.4 m s^{-1}. (b) From top to bottom: z_s, u, v, and h.

[33] As Table 1 shows, the height of the incident waves H^0_{rms} has a strong influence on the initial growth rate of instabilities σ_1 for both normal and oblique waves. Basically, the increase of the incident wave height leads to a strong increase of the initial growth rate. This agrees with previous modelling studies *Calvete et al.* [2005] and are realistic as all the experiments are done for mild wave conditions that are well below fully dissipative conditions. For waves of 0.8 m, the computed growth rate is (almost) nought. This wave height can define a boundary between low- and mild-energetic-wave conditions. For waves of 1.2 m, the growth saturation is not reached for oblique waves because the bar amplitude at the coastline tends to exceed the water depth, and this causes model overflow. However, information on the initial predominant mode can be obtained (σ_1, λ_1 and c_1), in particular, bars migrate quicker because of a stronger ambient current (Figure 2a). Higher waves are not considered because of the chosen model domain which ends at 4.5 m depth. They would have corresponded to conditions too energetic for the present model parameterization, particularly for the sediment transport formulation. We also notice a slight increase of the bar wavelength with the wave height, but only for normal waves.

[34] The variation of the wave period T of ±20% has almost no influence for normal waves, except that the bar amplitude A_{max} decreases slightly when T decreases and the growth rate σ_1 varies slightly. The same behavior for A_{max} and σ_1 is observed in the case of oblique waves. Moreover, the initial bar wavelength λ_1 does not depend on the wave period. However, by comparing the entire evolutions, when T increases, the minimum (maximum) bar wavelength λ_{min} (λ_{max}) decreases (increases). The higher the difference $\lambda_{max}-\lambda_{min}$ is, the more merging/splitting will occur so that this quantity is useful to measure the nonlinear character of the beach system. As shown by comparing the time evolution for $T = 6$ s and $T = 7.5$ s (Figures 7e–7h and 7a–7d), respectively), the nonlinear character of the system is strongly dependent on the wave period and decreases when T increases. A possible mechanism is discussed in 5.1

[35] As the linear theory suggests *Calvete et al.* [2005], the growth rate of the initial mode σ_1 decreases when the wave angle increases. For $\theta^0 \geq 7°$, the beach appears stable. In addition, the initial wavelength and migration velocity increase with θ^0. Interestingly, the final bar amplitude does not exactly follow the same behavior as the initial growth rate: it increases when θ^0 increases from 0 to 3°, and decreases for a further increase of θ^0. Moreover, neither the minimum nor the maximum wavelengths have a monotonic behavior. By looking at the difference, the strongest nonlinear character occurs for $\theta^0 = 3°$. This study of variation in wave angle does not pretend to be representative of and to be applicable to a real event for two reasons. Firstly, we consider an increment in wave angle of only 1° while in the field, buoys do not reach this accuracy. However, we show that a little change can considerably affect both the linear and the nonlinear regime of rhythmic bars. Also note that the incident wave angles are given at 4.5 m depth, thus they correspond to larger offshore angles and increments. Secondly, in nature, waves are not unidirectional but contain some spread. This has been investigated by *Reniers et al.* [2004], who shows that even a small amount of directional spreading can force the beach system in reaching a different wavelength. The present work aims to study the self-organization of a beach under hypothetical constant conditions, without introducing any wavelength forced by the waves.

[36] This sensitivity analysis is only use full for this particular experiment: for wave conditions given at the offshore model boundary (at 4.5 m depth) and for a particular alongshore bar shape, location and amplitude that affect the instability of the beach [*Calvete et al.*, 2007]. In

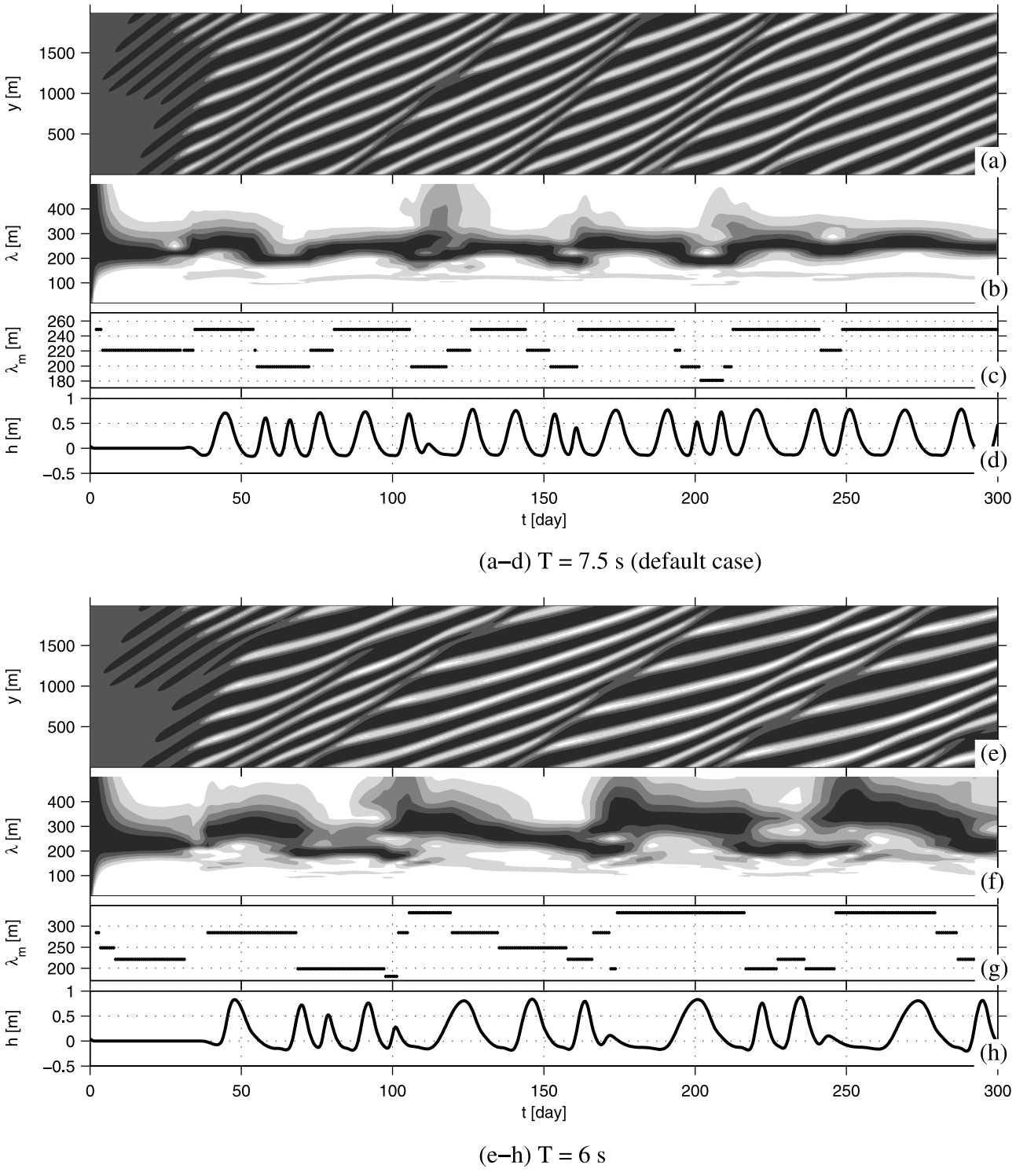

Figure 7. Oblique wave incidence. Time series. (a–d) $T = 7.5$ s (default case). (e–h) $T = 6$ s. (a, e) $h(x = 50$ m, $y, t)$, (b, f) $F(x = 50$ m, $\lambda, t)$, (c, g) $\lambda_m(x = 50$ m, $t)$, and (d, h) $h(x = 50$ m, $y = 1000$ m, $t)$. For a more precise description, see Figure 4 (a–d).

order to extend this analysis to a more general case, we introduce the nondimensional parameter γ_b that is the relative wave height where the wave energy dissipation on the longshore bar is maximum. Although close to the shoreline the relative wave height can reach 0.8, it never exceeds 0.5 over the bar. This means that the waves are breaking on the bar without transforming themselves in turbulent bores [*Masselink and Kroon*, 2006]. The range of γ_b is small (0.43–0.50), but below 0.4, the beach is stable. The highest instability (i.e., strongest growth rate) is found for $\gamma_b = 0.5$. However, this parameter is not sufficient to

Table 1. Parametric Trends[a]

	θ^0, deg	H_{rms}^0, m	T, s	x_b, m	γ_b	A_{max}, m	σ_1, /d	λ_1, m	c_1, m/d	λ_{min}, m	λ_{max}, m	c_{min}, m/d
H_{rms}^0		**0.8**		82	0.43	0.08	0.04	180	0	180	180	0
	0	***1.0***	*7.5*	*86*	*0.48*	*0.49*	*0.58*	*180*	*0*	*180*	*180*	*0*
		1.2		89	0.50	0.86	1.10	200	0	200	200	0
		0.8		82	0.43	0	...	...	...	...	...	...
	4	***1.0***	*7.5*	*86*	*0.48*	*0.54*	*0.24*	*220*	*27.8*	*180*	*250*	*14.0*
		1.2		89	0.50	1.1+	0.64	220	48.8	×	×	×
T			**6.0**	86	0.45	0.54	0.54	180	0	180	180	0
	0	*1.0*	***7.5***	*86*	*0.48*	*0.49*	*0.58*	*180*	*0*	*180*	*180*	*0*
			9.0	85	0.50	0.44	0.55	180	0	180	180	0
			6.0	86	0.45	0.65	0.20	220	25.3	180	320	8.2
	4	*1.0*	**7.5**	*86*	*0.48*	*0.54*	*0.24*	*220*	*27.8*	*180*	*250*	*14.0*
			9.0	85	0.50	0.44	0.20	220	31.0	200	250	21.0
θ^0	***0***			86	0.48	*0.49*	*0.58*	*180*	*0*	*180*	*180*	*0*
	1			86	0.48	0.52	0.55	180	7.4	180	220	3.7
	2			86	0.48	0.56	0.48	180	15.4	180	220	6.8
	3			86	0.48	0.58	0.36	200	22.0	165	280	9.3
	4	*1.0*	*7.5*	*86*	*0.48*	*0.54*	*0.24*	*220*	*27.8*	*180*	*250*	*14.0*
	5			86	0.48	0.50	0.22	250	35.7	220	280	22.0
	6			86	0.48	0.40	0.03	250	37.8	250	280	30.1
	7			86	0.48	0	...	...	...	...	...	...

[a]Effect of the variation of the initial wave height H_{rms}^0, the wave period T, and the initial wave angle θ^0 on the beach instabilities. x_b is the cross-shore position of the maximum wave energy dissipation on the longshore bar. γ_b is the relative wave height for $x = x_b$, i.e., $\gamma_b = H(x_b) / D(x_b)$. A_{max} is the bar amplitude at the final state, and σ_1, λ_1, and c_1 are the initial growth rate, the wavelength, and the migration celerity, respectively, corresponding to the initial predominant mode. λ_{min} is the minimum wavelength obtained during all the evolution. λ_{max} is the maximum wavelength, and c_{min} is the associated migration celerity. Italic font is used for the default cases. The cross symbol corresponds to the case where the bar saturation is not obtained. The plus symbol means that the value was increasing when the model stopped.

predict if the beach is unstable, as, among others, it is invariant with the offshore wave angle.

4. Physical Mechanisms

[37] The analysis of the mechanisms behind the growth of rhythmic bars as a self organization process has been made following previous studies *Falqués et al.* [2000]; *Coco et al.* [2002]; *Caballeria et al.* [2002]; *Ribas et al.* [2003]; *Calvete et al.* [2005] and *Garnier et al.* [2006a]. The analysis of the spatial distribution of (1) the potential stirring C (in particular, its profile at the basic state) and (2) the cross-shore component u of the velocity, provide the clue to understand the growth mechanisms. To understand the importance of the variable C, we introduce the bed evolution equation, "BEE", which can be derived from (5) and (1) by making the hypothesis of (1) $C \ll 1$ and (2) $|\partial D/\partial t| \simeq |\partial h/\partial t|$. Thus the BEE reads [*Garnier et al.*, 2006a]:

$$\frac{\partial h}{\partial t} \simeq \vec{\nabla}\cdot\left(\Gamma\vec{\nabla}h\right) - D\vec{v}\cdot\vec{\nabla}C \ , \tag{9}$$

where $\Gamma = \gamma\,\alpha\,u_b$ is called the morphodynamical diffusivity. Indeed, if the last term on its right-hand side is ignored, the BEE (9) becomes a diffusion equation. Notice that the first hypothesis (1) to lead to the BEE can be checked in Figure 2b which shows that $C < 10^{-3}$. The second hypothesis (2) is made by supposing that the effects of infragravity waves on sediment transport are neglected. This has been verified by running the model in the hydrodynamical mode (by disconnecting the sediment mass equation); even for a perturbed bathymetry, a stable hydrodynamical equilibrium state is reached, similar to the basic state.

[38] In the next part of this section, the BEE (9) will be analyzed for normal wave incidence and oblique wave incidence in order to understand the emergence of rhythmic features. This is based on the analysis made by *Garnier et al.* [2006a].

4.1. Normal Wave Incidence

[39] For normal wave incidence, at the initial step of the formation of rhythmic features, the alongshore gradient of the potential stirring is small compared to the cross-shore gradient. Thus the BEE (9) becomes:

$$\frac{\partial h}{\partial t} \simeq \vec{\nabla}\cdot\left(\Gamma\vec{\nabla}h\right) - D\,u\frac{\partial C}{\partial x} \tag{10}$$

[40] Because the first term in the right hand side of (90) is a diffusive term, the instability mechanism is governed by the sign of $u\,\partial C/\partial x$. In particular, two instability conditions can occur: (1) accretion ($\partial h/\partial t > 0$, i.e., $u\partial C/\partial x < 0$) over a shoal and (2) erosion ($\partial h/\partial t < 0$, i.e., $u\partial C/\partial x > 0$) in a trough. The analysis of the cross-shore profile of C at the basic state is therefore essential. As shown in Figures 2b and 8a, the cross-shore gradient of C is positive in the inner part of the longshore bar (50 m $< x <$ 80 m) while it is negative in the outer part ($x >$ 80 m). Thus instability can occur if (1) $u < 0$ (onshore oriented current) over a shoal and (2) $u > 0$ (offshore oriented current) over a trough in the inner zone. In the outer zone the instability requires the opposite cross-shore velocity direction: (1) $u > 0$ over a shoal and (2) $u < 0$ over a trough.

[41] The emergence of rhythmic features occurs if a positive feedback between the beach morphology and the hydrodynamics is established. In the surf zone, because of the increased (decreased) wave breaking and wave setup over the shoals (troughs), we observe the following behavior of the current: given a single fixed alongshore series of

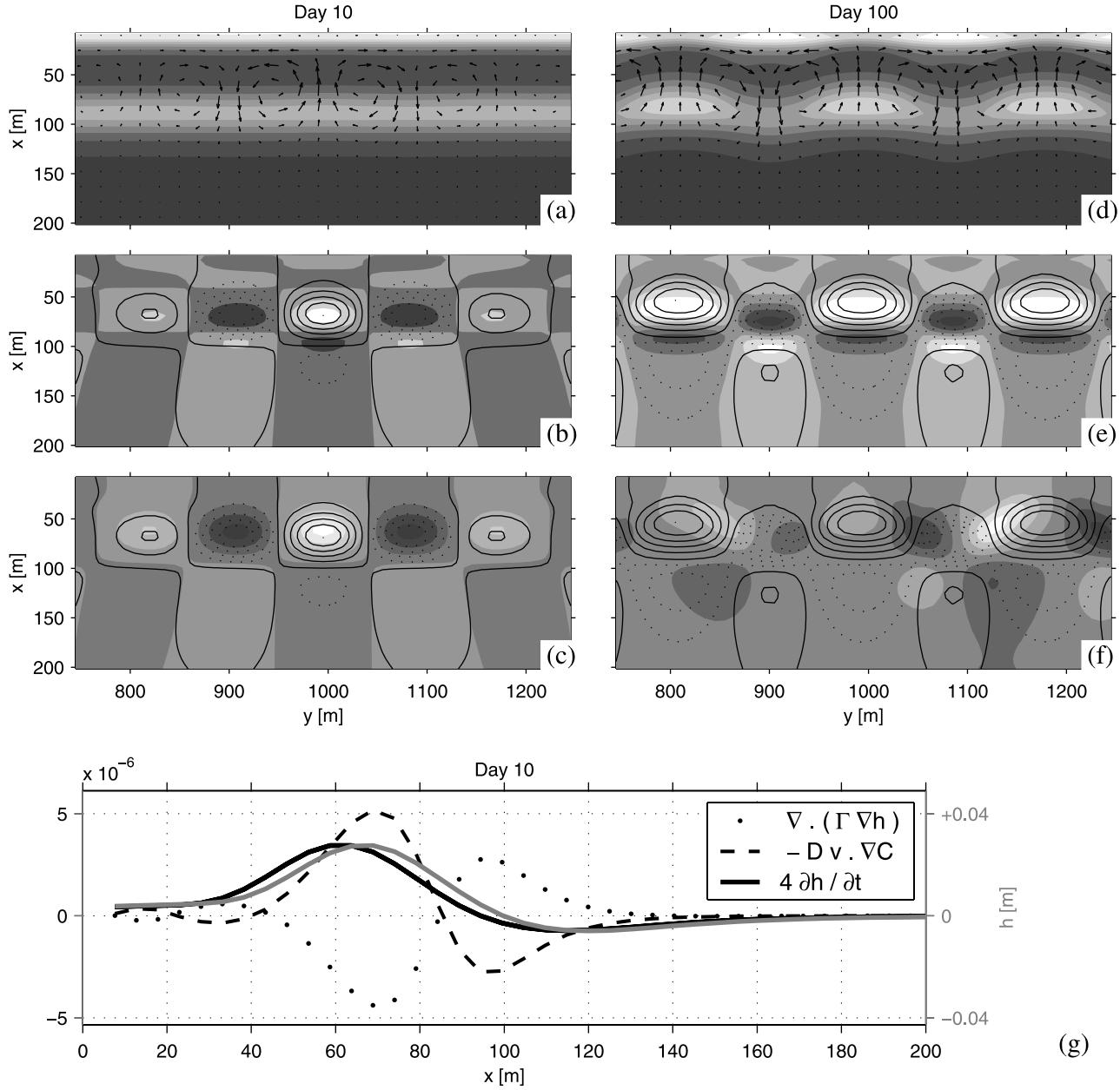

Figure 8. Normal wave incidence. Left (a–c): initial state. Right (d–f): final state. (a, d) C (small values are shaded, and large values are white) and current vectors. (b, e) $D\vec{v} \cdot \vec{\nabla} C$ (negative values (accretion) are white, and positive values (erosion) are shaded) and bottom perturbation (h) contours (crests are straight line, and troughs are dotted line). (c, f) $\partial h/\partial t$ (positive values (accretion) are white, and negative values (erosion) are shaded) and bottom perturbation (h) contours. (g) Cross-shore sections for $y = 1000$ m and $t = 10$ days. Gray line (right axis): bottom perturbation h in meters. Black lines (left axis): variables representing accretion (positive values) and erosion (negative values) in m s^{-1}. Black dotted line: $\vec{\nabla} \cdot (\Gamma\ \vec{\nabla}\ h)$. Black dashed line: $-D\ \vec{v} \cdot \vec{\nabla}\ C$. Black thick line: $\partial h/\partial t \simeq \vec{\nabla} \cdot (\Gamma\ \vec{\nabla}\ h) - D\ \vec{v} \cdot \vec{\nabla} C$.

shoals and troughs at any cross-shore location, the circulation is characterized by an onshore flow over the shoals and an offshore flow over the troughs [“Flow Over Topography” problem *Falqués et al.*, 2000]. Here, the assumption of irregular waves is made by considering the wave breaking dissipation parameterization of *Thornton and Guza* [1983]. The waves start to break far offshore, and, in particular from the offshore boundary of our domain, in other words, the studied domain is entirely within the surf zone. Thus instability only occurs at a cross-shore location where C increases offshore. The positive feedback is therefore established in the inner part of the longshore bar, by the so-called “bed surf mechanism” [*Falqués et al.*, 2000]. On the contrary, a negative feedback is expected in the outer zone (decreasing offshore potential stirring).

[42] However, the current circulation over the inner features extends offshore. Therefore the outer features can emerge, in antiphase with the inner ones because of the

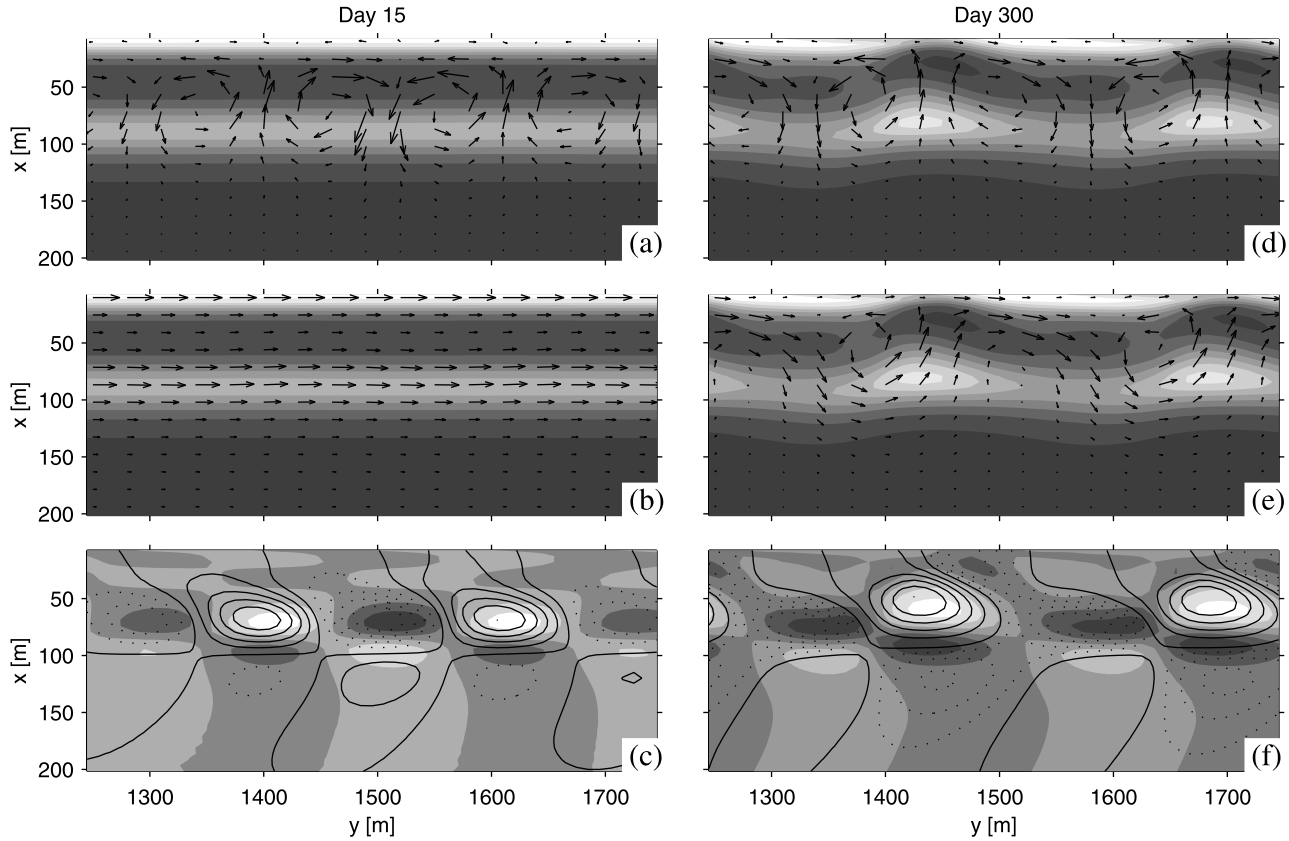

Figure 9. Oblique wave incidence. Left: initial state. Right: final state. (a, d) C (small values are shaded, and large values are white) and current perturbation vectors. (b, e) C (small values are shaded, and large values are white) and current vectors. (c, f) $D\vec{v} \cdot \vec{\nabla} C$ (negative values (accretion) are white, and positive values (erosion) are shaded) and bottom perturbation (h) contours (crests are straight lines, and troughs are dotted lines).

offshore decreasing potential stirring, and with a circulation the opposite of what would be expected on the basis of hydrodynamics alone without the presence of the inner features. The formation of the outer features is therefore forced by the inner system and is weaker because of a weaker current in the outer zone (Figures 8a and 8b). Thus a crescentic system can develop and has a smaller amplitude in the outer zone.

[43] The previous barred beach instability studies for irregular waves explain the formation of the crescentic system by analogy with the work on planar beach *Falqués et al.* [2000]. For random waves, crescentic bars do not appear on planar beach [*van Leeuwen et al.*, 2006; *Garnier*, 2007]. Nevertheless, by considering regular waves [*Falqués et al.*, 2000; *Caballeria et al.* 2002; *Ribas et al.*, 2003; *van Leeuwen et al.*, 2006], the single breaking point causes a peak in the potential stirring profile which is reminiscent of the present case of random waves on a barred beach. However, in the planar beach studies, the decreasing part of C corresponds to a nonbreaking zone. Thus, contrary to the present case, there is no negative feedback to counteract the formation of the outer features. This can explain why the outer features are less pronounced for random waves/barred beach than regular waves/planar beach.

[44] Another characteristic of the obtained rhythmic features has been the emergence of large-scale transverse bars (with small amplitude) in phase with the inner crests (Figure 3b). The analysis of the instability term $\vec{\nabla} C$ does not predict such patterns (Figure 8b). In particular, the gradient of the potential stirring is negative for 10 m $\leq x \leq$ 40 m. For 25 m $\leq x \leq$ 40 m, the current direction is forced by the inner crescentic bars, the predicted features should be in antiphase with them. For 10 m $\leq x \leq$ 25 m, because of the secondary circulation, other bed forms could appear, in phase with the inner crescentic bars. However, because this secondary circulation has a very low intensity, this area seems almost stable. Moreover, by analyzing the effective accretion/erosion patterns at this time step, i.e., $\partial h/\partial t$ (Figure 8c), we see the tendency of the large-scale transverse bars to form in phase and connected with the inner crescentic system. Thus the antiphase system predicted by the instability term for 25 m $\leq x \leq$ 40 m does not appear, and the predominant effect seems to be given by the bedslope transport.

[45] Figure 8g shows cross-shore profiles at the middle of the domain (y = 1000 m) which represent the tendency of accretion/erosion ($\partial h/\partial t$) and the contribution of the advective term $-D\,\vec{v} \cdot \vec{\nabla} C$, and the bedslope term $\vec{\nabla} \cdot (\Gamma \vec{\nabla} h)$, by keeping in mind the BEE (10): $\partial h/\partial t \simeq \vec{\nabla} \cdot (\Gamma \vec{\nabla} h) - D\,\vec{v} \cdot \vec{\nabla} C$. By comparing $\partial h/\partial t$ and h (gray line), we see the clear onshore migration (and growth) of the crescentic bar, for 25 m $\leq x \leq$ 110 m. By analyzing the correlation of both the advective term and the bedslope term with h (not shown), we conclude that the onshore migration is due globally (i.e., over 25 m $\leq x \leq$ 110 m) to the current, even if, in some

location (e.g., over 25 m $\leq x \leq$ 40 m), it is due to the bedslope term.

[46] The analysis of Figure 8e confirms this latter hypothesis, indeed the instability term $\vec{\nabla}C$ predicts mild erosion shoreward of each inner crest where Figure 3b exhibits a crest.

[47] At the final state (Figures 8d–8f), the equilibrium is maintained because of the bed slope transport. Indeed, Figure 8e still predicts instability whereas an equilibrium is reached. Even if this equilibrium is dynamical, i.e., $\partial h/\partial t \neq 0$ (Figure 8f), because the bars slightly oscillate, we show that the plots of $\vec{\nabla}C$ and $\partial h/\partial t$ do not fit.

4.2. Oblique Wave Incidence

[48] For oblique waves, the approximations made to derive the equation (10) are no longer valid because of the presence of the ambient longshore current. If we denote $V = V(x)$, the value of the longshore current at the basic state, the BEE (9) can be approximated as [*Garnier et al.*, 2006a]:

$$\frac{\partial h}{\partial t} \simeq \vec{\nabla}\cdot\left(\Gamma\vec{\nabla}h\right) - D\,u\frac{\partial C}{\partial x} - D\,V\frac{\partial C}{\partial y}\ . \qquad (11)$$

[49] As suggested by the linear stability analysis *Falqués et al.* [2000], the second term in the right hand side of equation (11) is mainly responsible for the growth of instabilities: Figures 9a and 9c show that the same kind of behavior as for normal waves occurs, with positive feedback associated with the increasing potential stirring. Therefore inner features appear and force the development of the outer features (in antiphase).

[50] One aspect of the bed features under oblique wave incidence is their migration with the longshore current. According to the previous studies *Falqués et al.* [2000]; *Ribas et al.* [2003]; *Garnier et al.* [2006a], this is caused by the last term of equation (11). For normal waves (nonmigrating bars), the maximum of deposition (erosion) occurs on the top of the bars (in the bottom of the troughs). For oblique waves, the ambient longshore current characterized by $V > 0$, causes a down-current shift of the maximum deposition/erosion patterns (Figure 9c). Indeed, the last term of the equation (11), $-D\,V\partial C/\partial y$, is maximum somewhat down current of the top of the shoal, i.e., where $\partial C/\partial y < 0$. On the other hand, the maximum erosion occurs somewhat down current of the bottom of the troughs.

[51] Finally, the large-scale transverse bar system appearing for normal waves develops with a down-current orientation for oblique waves. Figure 9c confirms the importance of the bedslope transport also in this case: the instability term $D\ \vec{v}\cdot\vec{\nabla}C$ does not explain the emergence of the morphological patterns appearing in the area $x < 50$ m, that are therefore also because of the term $\vec{\nabla}\cdot(\Gamma\vec{\nabla}h)$.

5. Discussion

5.1. Nonlinear Dynamics

[52] One of the most important goals of this nonlinear modelling study has been to follow the development of rhythmic features from an initially uniform alongshore bar that is unstable to a nonlinear regime. The main advantage of nonlinear versus linear stability analysis is the possibility of simulating the finite amplitude dynamics and not only the tendency of the bar to grow. However, for numerical reasons, previous nonlinear studies stopped the evolution while the bars were still growing. Here the saturation of the bed form growth has been obtained. It can be explained by the same mechanisms as for transverse bars [*Garnier et al.*, 2006a], resulting from a balance between the positive feedback flow/morphology and the bedslope sediment transport.

[53] For the first time, thanks to the saturation process, the amplitude of crescentic bars can be quantified with a numerical model. For most of the experiments, the bed forms reach a maximum amplitude at a certain time (that is not necessarily the final time). The maximum height (maximum vertical distance between crest and trough, i.e., twice the maximum amplitude) obtained is about 2 m, excluding the experiments leading to model overflow. This work shows a limitation of linear stability analysis and nonlinear studies that only show the growing processes of the bed forms. Here, we demonstrate the importance of the nonlinear regime analysis to determine how much the bar will grow. Indeed, it appears that both the final and the maximum bar amplitude are not entirely related to the initial growth rate of the bed forms, neither for the initial mode nor for any other modes. The bar amplitude also depends on the shape of the bars and in particular on their asymmetry (e.g., narrow channels and large crests) that allows the growth saturation through the increasing bedslope transport. For example, for a given wave period and incident wave height, we observed the typical decrease in growth rate of instabilities when the wave incidence angle increases [as, for instance, *Castelle*, 2004; *Calvete et al.*, 2005], however, the maximum bar amplitude is obtained not for normal wave incidence but for a slight obliquity ($\theta = 3°$ at $x = 250$ m).

[54] As shown in the presented simulations, the dynamics of the beach can be strongly nonlinear, not only by the asymmetry of the final beach state (bed forms, jet-like rip currents…), but also by the merging/splitting that can occur during the evolution of the bars even for constant incoming wave height. Therefore previous studies on the initial steps of beach evolution predict the predominant wavelength that will first emerge, but disregard if the wavelength changes in time. In some experiments, as for instance in the presented normal wave incidence simulations, we do not observe any merging/splitting in bars. Thus the predominant mode is the same for the formation of features and for the nonlinear evolution. However, for most of the oblique wave experiments, the wavelength changes in time, and merging eventually dominates splitting so that the final wavelength is larger than the initial one. During beach evolution, we observe a range between the minimum and the maximum wavelength ($\lambda_{max}/\lambda_{min}-1$) up to 70%. This quantity characterizes the nonlinear character of the beach system. The field study from *van Enckevort et al.* [2004] shows that the change in wavelength results from temporal variability in the wave forcing. The present study agrees as different wavelengths are obtained depending on the applied wave conditions. However, we show here that this change can occur because of different mechanisms, as we observe merging/splitting under constant wave forcing, if the event

is sufficiently long, e.g., well formed rhythmic bars can a merge or split in approximately 10 days of constant waves.

[55] Linear stability analysis [*Calvete et al.*, 2005] predicts that, for normal wave incidence, the initial wavelength increases or is the same for a higher-incident wave action ($\sim T\, H^0_{\mathrm{rms}})^2$. This can be explained by stronger gradient in potential stirring for higher or longer waves (see *C* profiles, Figure 2b). For oblique waves, while an increase in wave height also leads to larger spacing of bars, the tendency was inverted when the wave period increases (see explanation of *Calvete et al.* [2005]). Here, because of the presence of the nonlinear terms, and, in particular, because of the fact that longer waves increase the diffusion of the bars (for instance, through the wave orbital velocity which acts on the downslope transport), the wave period does not affects the initial bar wavelength.

[56] Actually, most of the dependence wave action/bar wavelength occurs in the nonlinear regime, depending if the bars merge, or not. The mechanisms are complex because of the competition between two opposite effects. When the wave height or the wave period are larger, the final bar spacing can (1) increase or (2) decrease, because of (1) larger gradients in potential stirring lead to larger-scale instabilities and also larger morphological diffusion, which tends to damp smaller bed forms; (2) the larger diffusion also reduces the nonlinear interactions, so less merging occurs and: wavelengths are reduced. We have not found a general rule explaining which from (1) and (2) dominates. It seems to depend on many factors such as wave angle and beach characteristics. Notice that mechanism (2) has not commonly been identified as it can only be observed in long-term evolution. An interesting example where it dominates over (1) is the case of increasing wave period from 6 s to 7.5 s which leads to no influence in initial spacing but leads to a decrease in final spacing of 30%. This has also been identified by *Garnier et al.* [2008a] in simulations on the Truc Vert beach, SW of France, for normal waves by varying the wave height: the initial bar wavelength is the same but the final one decreases for higher waves.

5.2. Dynamical Equilibrium

[57] As previously said, the saturation of the growth of the instabilities has been reached in most of the experiments by a balance between production (positive feedback) and damping (downslope transport). Moreover, it has been found that this balance stabilizes in time; this shows that an equilibrium has been reached. The results given for the final state correspond to the morphology at the equilibrium state. We qualify this equilibrium as 'dynamical' because the bars can still be in movement whereas the balance is stabilized. For instance for oblique waves the longshore current induces the migration of bars, thus, at the equilibrium bars are advected down current. Even without migration (i.e., for normal wave incidence) the evolution of the bars may not stop at the equilibrium, because they can oscillate between distinct states.

[58] This equilibrium state is characterized by a particular morphology which consists of, for normal waves, a kind of (large-scale) transverse bar. This beach configuration is reminiscent of the TBR (Transverse Bar and Rip) state defined by [*Wright and Short*, 1984]. For oblique waves, the rhythmic features take an oblique down-current orientation, similar to the large-scale oblique bars observed on the French Aquitanian coast *Lafon et al.* [2002]. Because the mechanisms of formation and the shape (length scale, cross-shore position) of the large-scale oblique/transverse bars are similar, it seems appropriate that they should both be classified as a TBR state.

[59] In agreement with the observation [*Wright and Short*, 1984; *Short*, 1999; *Plant et al.*, 2006, 2008], the transition between an alongshore uniform barred beach state ("LBT", "Longshore Bar and Trough") and the TBR obtained at the equilibrium state is not straightforward: there is a transient state composed by crescentic bars. This is reminiscent of the RBB state (Rhythmic Bar and Beach), although the megacusps are not explicitly observed in the present simulations. Thus this study shows that the transitions LBT → RBB → TBR can happen by self-organization mechanisms from 2DH morphodynamical processes without considering an explicit cross-shore sediment transport.

5.3. Limitations of the Study and Further Work

[60] Here we assume that the alongshore averaged cross-shore beach profile is stable, resulting from an equilibrium between the onshore sediment transport (e.g., because of wave skewness) and the offshore sediment transport (because of undertow and beach slope). This hypothesis remains valid as long as bed surf/bed flow processes are faster than the cross-shore processes (formation and moving of a longshore bar). The above three different beach states were obtained under this hypothesis but results would probably be more realistic by relaxing this assumption. For instance, one aspect of the bars at the described equilibrium state which differs from the TBR state of *Short* [1999] is that their maximum amplitude is at their tip, while it seems to be on the coastline in nature. The cross-shore migration of the longshore bar could explain this discrepancy. The integration of cross-shore sediment transport has been investigated in the recent study of *Dronen and Deigaard* [2007] by using a quasi three-dimensional model, showing the formation of an alongshore bar and then of rhythmic features, from an initially planar beach profile. However, they found that the generation of the crescentic features is associated with offshore bar migration. That is the opposite of what happens in nature. Another cross-shore mechanism explaining the shoreward migration of the bars can be associated with surf zone bores. When propagating over a longshore bar, they take sediment from the seaward side of the bar and deposit it on the landward side. This mechanism has been identified in field studies on the intertidal zone [*Kroon and Masselink*, 2002; *Houser et al.*, 2006; *Masselink and Kroon*, 2006], and can therefore be relevant in the transition RBB → TBB.

[61] Thus in this modelling study, the 1D processes, i.e., the processes that govern onshore or offshore migration of an alongshore uniform bar, are neglected, but this does not mean that there is not cross-shore transport, locally. Indeed, the formation of the crescentic bar system (LBT → RBB) is due to a positive feedback between the 2D current circulation and the morphological response (bed surf mechanism) but can also be interpreted as a local onshore transport occurring over each crest of the crescentic system associated with onshore current that takes the offshore sediment (in the corresponding outer trough) and bring it shoreward (over

the inner crest). This local cross-shore process is due to the advective part ($\alpha\vec{v}$) of our sediment transport formula which contributes, alone, to the instability. To explain the further attachment of the system to the coastline (RBB → TBB), we show that, not only the advective part plays a role, but also the diffusive part, i.e., the bedslope transport ($\alpha\ \gamma\ u_b\ \vec{\nabla}\ h$).

[62] This transport contributes to both the saturation of the growing features and to their final shape. One limitation of this work comes from the simplicity of the diffusive transport formulation and from the uncertainty in the bedslope coefficient γ. Until now, no formula has been validated in the field because of the difficulty of sediment transport measurement in the surf zone during strong and long events leading to morphological instabilities. Numerical modelling allow us to check the sensitivity of the results on the parameter γ. We obtain the growth and the saturation of rhythmic features with similar shape for $3 < \gamma < 7$. For larger values, the beach is stable. For lower values, the model overflows, but the initial wave length and its corresponding growth rate can be determined ($\lambda_1 = 180$ m, $\sigma_1 = 0.58$ day^{-1}, for the default case under normal wave incidence). The initial wave length can change by ±20% with respect to the default case (165 m $< \lambda_1 <$ 220 m) and the initial growth rate can be up to $\sigma_1 = 2.0$ day^{-1} (for $\gamma = 1$), thus we remain in the same order of magnitude.

[63] The modelling study of *Ranasinghe et al.* [2004] applied to the observed RBB → TBB transition in Palm Beach, Australia differs from the present study. Firstly because of their initial condition, particularly their initial topography is not reached from self-organization by the model, but is taken from preexisting RBB state based on Argus images. Secondly their model parameterization differs mainly because of the use of regular waves and of the Bailard's sediment transport formula. Even if they explain the shore attachment from cross-shore processes, a detailed analysis of the different terms in the sediment transport formulation is not given. It should be added that they do not include 1D processes either, their analysis is therefore local and comparable to our analysis of the advective transport.

[64] Even if their model is not validated at the previous morphological state as they cannot reach the transition LBT → RBB, the comparison of modelling/observations during the RBB → TBB, is successful and would be due to an onshore migration of the crescentic system occurring for a decline in wave energy. This is consistent with our theory of formation of crescentic system around a longshore line located at the cross-shore position of the maximum in potential stirring C at the basic state (section 4.1). Indeed, for a decreasing incident wave height, the maximum in C will be shifted cross-shore, thus, the crescentic system would tends to migrate shoreward. However, this does not happen in our configuration because the use of random waves together with our particular beach profile do not allow a large enough shift in the maximum of C. The 1D cross-shore processes that cause onshore migration of the longshore bar could be the missing point, as they would cause the increase of this shift.

[65] As with the previous models used to study the emergence of bed instabilities in the surf zone, the present model is highly simplified because of the averaging and the parameterization of many processes. The wave forcing and the initial topography used for our experiments are also very idealized. Firstly a (strong) constant wave forcing of 1 m waves imposed for up to 300 days of beach evolution is highly improbable. However, it is important to see that such hypothetical conditions lead to an equilibrium state by 2DH processes. Secondly this almost alongshore uniform initial topography of 0.5 km^2 perturbed by an idealized bump of only 1.5 m^3 of sand mostly explains the reason of the very long growth times obtained in our simulations (∼20 days). The growth time depends on the initial conditions, in particular on the volume of the initial bed perturbation, and on its shape. In reality the beach is never alongshore uniform, in particular because of ripples or preexisting random features, but also because of preexisting rhythmic features. Therefore the *e*-folding time (inverse of the growth rate) is a more meaningful measure of how vigorous is the growth of features. Here this is the order of ∼1 day. This means, for instance, that an initial preexisting rhythmic topography with bars of 20 cm high, will grow up to 55 cm after 1 day.

6. Conclusion

[66] The long-term evolution of rip channel systems emerging from the deformation of a longshore bar is simulated with a numerical model. The model is based on a wave- and depth-averaged shallow water equation solver with wave driver, sediment transport and bed updating. It is applied to study the (in)stability of an initially alongshore uniform single-barred beach under constant offshore wave conditions.

[67] We identify two distinct regimes in the morphological evolution of the rip channels. (1) The linear regime is characterized by crescentic bar systems that emerge as a free instability of the coupling between topography, waves and current. The results are consistent with those from linear stability analysis. (2) The nonlinear regime is where the bed forms become asymmetric, merge and split, and their growth saturates.

[68] In this regime the initial crescentic bar systems reorganize to form large-scale transverse or oblique bar systems, for normal or oblique wave incidence, respectively. Thus the basic morphological transitions ''LBT'' → ''RBB'' → ''TBR'' (Longshore Bar and Trough → Rhythmic Bar and Beach → Transverse Bar and Rip) described by earlier conceptual models (based on observation) are here reproduced in finite amplitude, notwithstanding excluding the cross-shore sediment transport due to wave asymmetry and undertow. Moreover these transverse/oblique bars are found to be a dynamical equilibrium state of the beach system.

[69] The study of the physical mechanisms allows us to understand their formation; in particular, the two parts of the sediment transport formula (advective and bedslope) have an important role: the advective part induces the instability and explains how the crescentic bars tend to force the formation of megacusps; the bedslope transport damps the instability. Both terms contribute to the attachment of the megacusps to the crescentic bars.

[70] The simulations have been done for different wave forcings (incident wave heights H^0_{rms}, wave periods T and wave angles θ^0). The initial growth rate σ_1 of the instabil-

ities is up to 1.1 day^{-1} and decreases with the incident wave obliquity; it is not necessarily related to the final height (from crest to trough) of the bars which is up to 2 m (found for σ_1 = 0.6 day^{-1}). The bar wavelength ranges between 165 m and 320 m. The variation in the initial bar wavelength is more dependent on θ^0 (40%) than on the incident wave action $\sim T\,(H^0_{\mathrm{rms}})^2$ (10%). However, a larger wavelength variation is obtained during a temporal evolution for steady wave conditions (70%). This reveals the importance of merging/splitting that is quantified by the ''nonlinear character'' of the beach system. The hypothesis of larger diffusivity creating larger features is no longer valid in the nonlinear evolution as the increase of diffusivity can in turn reduce the nonlinear character, i.e., reduce the merging of the bars.

[71] **Acknowledgments.** This research is part of the PUDEM project, which is funded by the Spanish Government under contract REN2003-06637-C02-01/MAR and of the CTM2006-08875/MAR project. It is also funded through the Ramón y Cajal contract of D. Calvete. The work of R. Garnier was supported by the University of Nottingham. Its support is gratefully acknowledged. We thank the two anonymous referees for their useful comments.

References

Battjes, J. A. (1975), Modeling of turbulence in the surfzone, in *Proc. Symp. Model. Tech*., pp. 1050–1061, Am. Soc. of Civ. Eng., New York.

Bowen, A. J., and D. L. Inman (1971), Edge waves and crescentic bars, *J. Geophys. Res.*, *76*(36), 8662–8671.

Caballeria, M., G. Coco, A. Falqués, and D. A. Huntley (2002), Self-organization mechanisms for the formation of nearshore crescentic and transverse sand bars, *J. Fluid Mech.*, *465*, 379–410.

Calvete, D., N. Dodd, A. Falqués, and S. M. van Leeuwen (2005), Morphological development of rip channel systems: Normal and near normal wave incidence, *J. Geophys. Res.*, *110*, C10006, doi:10.1029/2004JC002803.

Calvete, D., G. Coco, A. Falqués, and N. Dodd (2007), (Un)predictability in rip channel systems, *Geophys. Res. Lett.*, *34*, L05605, doi:10.1029/2006GL028162.

Castelle, B. (2004), Modélisation de l'hydrodynamique sédimentaire audessus des barres sableuses soumises à l'action de la houle: Application à la côte aquitaine, Ph.D. thesis, Université Bordeaux I, France.

Castelle, B., P. Bonneton, H. Dupuis, and N. Senechal (2007), Double bar beach dynamics on the high-energy meso-macrotidal French Aquitanian coast: A review, *Mar. Geol.*, *245*, 141–159.

Christensen, E., R. Deigaard, and J. Fredsoe (1994), Sea bed stability on a long straight coast, in *Coastal Eng. 1994*, vol. 4, edited by B. L. Edge, pp. 1865–1879, Am. Soc. of Civ. Eng., Reston, Va.

Coco, G., M. Caballeria, A. Falqués, and D. H. Huntley (2002), Crescentic bars and nearshore self-organization processes, in *Coastal Eng. 2002*, vol. 3, edited by J. M. Smith, pp. 3765–3777, Am. Soc. of Civ. Eng., World Scientific, River Edge, N.J.

Damgaard, J., N. Dodd, L. Hall, and T. Chesher (2002), Morphodynamic modelling of rip channel growth, *Coastal Eng.*, *45*, 199–221.

De Melo Apoluceno, D. (2002), Morpho-hydrodynamique des plages à barres en domaine méso à macro-tidal: Exemple de la plage du truc vert, gironde, france, Ph.D. thesis, Université Bordeaux I, France.

De Melo Apoluceno, D., H. Howa, H. Dupuis, and G. Oggian (2002), Morphodynamics of ridge and runnel systems during summer, *J. Coastal Res.*, *36*, 222–230, Special Issue.

Deigaard, R., N. Drnen, J. Fredsoe, J. H. Jensen, and M. P. Jrgesen (1999), A morphological stability analysis for a long straight barred coast, *Coastal Eng.*, *36*(3), 171–195.

Dronen, N., and R. Deigaard (2007), Quasi-three-dimensional modelling of the morphology of longshore bars, *Coastal Eng.*, *54*, 197–215.

Evans, O. F. (1938), The classification and origin of beach cusps, *J. Geol.*, *46*, 615–627.

Falqués, A. (1989), Formación de topografí tmica en el Delta del Ebro, *Rev. Geofis.*, *45*(2), 143–156.

Falqués, A., A. Montoto, and V. Iranzo (1996), Bed-flow instability of the longshore current, *Cont. Shelf Res.*, *16*(15), 1927–1964.

Falqués, A., G. Coco, and D. A. Huntley (2000), A mechanism for the generation of wave-driven rhythmic patterns in the surf zone, *J. Geophys. Res.*, *105*(C10), 24,071–24,088.

Garnier, R. (2007), Nonlinear modelling of surf zone morphodynamical instabilities, Ph.D. thesis, Appl. Physics Dept., Univ. Politècnica de Catalunya, Barcelona, Spain.

Garnier, R., D. Calvete, A. Falqués, and M. Caballeria (2006a), Generation and nonlinear evolution of shore-oblique/transverse sand bars, *J. Fluid Mech.*, *567*, 327–360.

Garnier, R., D. Calvete, A. Falqués, and M. Caballeria (2006b), Modeling ridge and runnel system development from an intertidal shore parallel bar, in *Coastal Eng. 2006*, pp. 2679–2690, edited by J. M. Smith, Am. Soc. of Civ. Eng., World Scientific, River Edge, N.J.

Garnier, R., P. Bonneton, A. Falqués, and D. Calvete (2008a), Modelling the formation and the nonlinear evolution of crescentic bars of the Aquitanian coast, *La Houille Blanche*, *3*, 33–38, doi:10.1051/lhb:2008024, in French.

Garnier, R., D. Calvete, N. Dodd, and A. Falqués (2008b), Modeling the interaction between transverse and crescentic bar systems, in *River, Coastal and Estuarine Morphodynamics: RCEM 2007*, vol. 2, edited by C. M. Dohmen-Jansen and S. J. M. H. Hulscher, pp. 931–937, Taylor and Francis Group, London.

Haller, M. C., R. A. Dalrymple, and I. A. Svendsen (2002), Experimental study of nearshore dynamics on a barred beach with rip channels, *J. Geophys. Res.*, *107*(C6), 3061, doi:10.1029/2001JC000955.

Holman, R. A., and A. J. Bowen (1982), Bars, bumps, and holes: Models for the generation of complex beach topography, *J. Geophys. Res.*, *87*(C1), 457–468.

Horikawa, K. (1988), *Nearshore Dynamics and Coastal Processes*, Univ. of Tokyo Press, Tokyo, Japan.

Houser, C., B. Greenwood, and T. Aagard (2006), Divergent response of an intertidal swash bar, *Earth Surf. Processes Landforms*, *31*, 1775–1791.

Klein, M. D., and H. M. Schuttelaars (2006), Morphodynamic evolution of double-barred beaches, *J. Geophys. Res.*, *111*, C06017, doi:10.1029/2005JC003155.

Komar, P. D. (1998), *Beach Processes and Sedimentation*, 2nd ed., Prentice Hall, Englewood Cliffs, N.J.

Konicki, K. M., and R. A. Holman (2000), The statistics and kinematics of transverse bars on an open coast, *Mar. Geol.*, *169*, 69–101.

Kroon, A., and G. Masselink (2002), Morphodynamics of intertidal bar morphology on a macrotidal beach under low-energy wave conditions, North Lincolnshire, England, *Mar. Geol.*, *190*, 591–608.

Lafon, V., H. Dupuis, H. Howa, and J. M. Froidefond (2002), Determining ridge and runnel longshore migration rate using spot imagery, *Oceanol. Acta*, *25*, 149–158.

Lafon, V., D. D. M. Apoluceno, H. Dupuis, D. Michel, H. Howa, and J. M. Froidefond (2004), Morphodynamics of nearshore rhythmic sandbars in a mixed-energy environment (SW France). I: Mapping beach changes using visible satellite imagery, *Estuarine, Coastal Shelf Sci.*, *61*, 289–299.

Lafon, V., H. Dupuis, R. Butel, B. Castelle, D. Michel, H. Howa, and D. D. M. Apoluceno (2005), Morphodynamics of nearshore rhythmic sandbars in a mixed-energy environment (SW france): 2. Physical forcing analysis, *Estuarine, Coastal Shelf Sci.*, *65*, 449–462.

Longuet-Higgins, M. S., and R. W. Stewart (1964), Radiation stresses in water waves: A physical discussion with applications, *Deep Sea Res.*, *11*, 529–562.

MacMahan, J. H., E. B. Thornton, T. P. Stanton, and A. J. H. M. Reniers (2005), RIPEX: Observations of a rip current system, *Mar. Geol.*, *218*, 113–134.

Masselink, G., and A. Kroon (2006), Morphodynamics of intertidal bars in wave-dominated coastal settings—a review, *Geomorphology*, *73*, 33–49.

Mei, C. C. (1989), *The Applied Dynamics of Ocean Surface Waves, Advanced Series on Ocean Engineering*, vol. 1, World Scientific, Singapore.

Niederoda, A. W., and W. F. Tanner (1970), Preliminary study on transverse bars, *Mar. Geol.*, *9*, 41–62.

Plant, N. G., K. T. Holland, and R. A. Holman (2006), A dynamical attractor governs beach response to storms, *Geophys. Res. Lett.*, *33*, L17607, doi:10.1029/2006GL027105.

Plant, N. G., K. T. Holland, R. A. Holman, K. D. Splinter, A. Reniers, and M. Smit (2008), A dynamical systems approach to analysing morphodynamic states, in *River, Coastal and Estuarine Morphodynamics: RCEM 2007*, vol. 1, edited by C. M. Dohmen-Jansen and S. J. M. H. Hulscher, pp. 217–221, Taylor and Francis Group, London.

Ranasinghe, R., G. Symonds, K. Black, and R. Holman (2004), Morphodynamics of intermediate beaches: A video imaging and numerical modelling study, *Coastal Eng.*, *51*, 629–655.

Reniers, A. J. H. M., J. A. Roelvink, and E. B. Thornton (2004), Morphodynamic modeling of an embayed beach under wave group forcing, *J. Geophys. Res.*, *109*, C01030, doi:10.1029/2002JC001586.

Ribas, F., and A. Kroon (2007), Characteristics and dynamics of surfzone transverse finger bars, *J. Geophys. Res.*, *112*, F03028, doi:10.1029/2006JF000685.

Ribas, F., A. Falqués, and A. Montoto (2003), Nearshore oblique sand bars, *J. Geophys. Res.*, *108*(C4), 3119, doi:10.1029/2001JC000985.

Ruessink, B. G., G. Coco, R. Ranasinghe, and I. L. Turner (2007), Coupled and noncoupled behavior of three-dimensional morphological patterns in a double sandbar system, *J. Geophys. Res.*, *112*, C07002, doi:10.1029/2006JC003799.

Short, A. D. (1999), *Handbook of Beach and Shoreface Morphodynamics*, Wiley, Chichester, U. K.

Soulsby, R. L. (1997), *Dynamics of Marine Sands*, Thomas Telford, London, U. K.

Thornton, B., and R. T. Guza (1983), Transformation of wave height distribution, *J. Geophys. Res.*, *88*(10), 5925–5938.

van Enckevort, I. M. J., B. G. Ruessink, G. Coco, K. Suzuki, I. L. Turner, N. G. Plant, and R. A. Holman (2004), Observations of nearshore crescentic sandbars, *J. Geophys. Res.*, *109*, C06028, doi:10.1029/2003JC002214.

van Leeuwen, S. M., N. Dodd, D. Calvete, and A. Falqués (2006), Physics of nearshore bed pattern formation under regular or random waves, *J. Geophys. Res.*, *111*, F01023, doi:10.1029/2005JF000360.

Wright, L. D., and A. D. Short (1984), Morphodynamic variability of surf zones and beaches: A synthesis, *Mar. Geol.*, *56*, 93–118.

Yu, J., and D. N. Slinn (2003), Effects of wave-current interaction on rip currents, *J. Geophys. Res.*, *108*(C3), 3088, doi:10.1029/2001JC001105.

D. Calvete and A. Falqués, Departament de Física Aplicada, Universitat Politécnica de Catalunya, Campus Nord-Modùl B4, 08034 Barcelona, Spain. (calvete@fa.upc.edu; falques@fa.upc.edu)

N. Dodd and R. Garnier, School of Civil Engineering, University of Nottingham, University Park, Nottingham NG7 2RD, UK. (nick.dodd@nottingham.ac.uk; roland.garnier@nottingham.ac.uk)